Published in final edited form as:
Nature. 2014 January 16; 505(7483): 412–416. doi:10.1038/nature12807.

Muc5b Is Required for Airway Defense

Michelle G. Roy[1,*], **Alessandra Livraghi-Butrico**[2,*], **Ashley A. Fletcher**[3,*], **Melissa M. McElwee**[1], **Scott E. Evans**[1], **Ryan M. Boerner**[4], **Samantha N. Alexander**[1], **Lindsey K. Bellinghausen**[1], **Alfred S. Song**[1], **Youlia M. Petrova**[1], **Michael J. Tuvim**[1], **Roberto Adachi**[1], **Irlanda Romo**[1,5], **Andrea S. Bordt**[6], **M. Gabriela Bowden**[6,7], **Joseph H. Sisson**[8], **Prescott G. Woodruff**[9], **David J. Thornton**[10], **Karine Rousseau**[10], **Maria M. De la Garza**[1], **Seyed J. Moghaddam**[1], **Harry Karmouty-Quintana**[4], **Michael R. Blackburn**[4], **Scott M. Drouin**[4], **C. William Davis**[2], **Kristy A. Terrell**[2], **Barbara R. Grubb**[2], **Wanda K. O'Neal**[2], **Sonia C. Flores**[3], **Adela Cota-Gomez**[3], **Catherine A. Lozupone**[3], **Jody M. Donnelly**[3], **Alan M. Watson**[3], **Corinne E. Hennessy**[3], **Rebecca C. Keith**[3], **Ivana V. Yang**[3], **Lea Barthel**[3,11], **Peter M. Henson**[3,11], **William J. Janssen**[3,11], **David A. Schwartz**[3], **Richard C. Boucher**[2], **Burton F. Dickey**[3], and **Christopher M. Evans**[1,3]

[1]University of Texas, MD Anderson Cancer Center, Houston, TX, 77030, USA

[2]University of North Carolina-Chapel Hill, Chapel Hill, NC, 27599, USA

[3]University of Colorado School of Medicine, Aurora, CO, 80045, USA

[4]University of Texas Health Science Center-Houston Medical School, Houston, TX, 77030, USA

[5]Instituto Tecnológico y de Estudios Superiores de Monterrey, Nuevo León, Mexico

[6] Texas A&M Health Science Center, Houston, TX, 77030, USA

[7]University of Houston-Downtown, Houston, TX, 77002, USA

[8]University of Nebraska Medical Center, Omaha, NE, 68198, USA

[9]University of California San Francisco, San Francisco, CA, 27599, USA

[10]Univeristy of Manchester, Manchester, M13 9PT, UK

[11]Natinoal Jewish Health, Denver, CO, 80206, USA

Corresponding Author: Christopher M. Evans, PhD, Department of Medicine, Division of Pulmonary Sciences and Critical Care, University of Colorado Denver School of Medicine, 12700 E 19th Avenue, Mailstop 8611, Aurora, CO, 80045, (303) 724-6573 [tele], Christopher.Evans@ucdenver.edu.

[*]**These authors contributed equally to this work.**

Author contributions

M.G.R., A.L.-B., and A.A.F designed and performed survival, histological, particle clearance, inflammation, and infectious agent identification experiments, performed and collected data for *S. aureus* infection, macrophage and neutrophil identification experiments, and cytokine analyses. A.M.W. R.C.K. C.E.H., and D.A.S. generated and assisted in studies in *Muc5b*^{Tg} mice. M.M.M., R.M.B, I.R., A.S.B., M.G.B., W.K.O., K.A.T., S.C.F., A.C.-G., J.A.D., and C.A.L. performed infectious pneumonia and infectious agent identification experiments. S.N.A., L.K.B., A.S.S., and Y.P. constructed and generated *Muc5b* knockout mice. S.E.E., M.M.D.G., S.J.M., and M.J.T. assisted in the design and performance of inflammation studies. B.R.G., R.A., H.K.-Q., and M.R.B. assisted in the design and performance of hypoxemia studies. J.H.S., S.M.D., and B.R.G. assisted in the design and performance of tracheal and nasal mucociliary function studies. D.J.T. and K.R. provided purified MUC5B protein. W.J.J. and L.B. designed and performed macrophage activation and apoptosis assays. I.V.Y, P.M.H., P.G.W., C.W.D., R.C.B, and B.F.D. assisted in the analysis and interpretation of data, and C.W.D. provided Muc5b antisera. C.M.E. designed the study, analyzed data, and wrote the manuscript.

Competing Interests

The authors have no competing interests to declare.

Abstract

Respiratory surfaces are exposed to billions of particulates and pathogens daily. A protective mucus barrier traps and eliminates them via mucociliary clearance (MCC)[1,2]. However, excessive mucus contributes to transient respiratory infections and to the pathogenesis of numerous respiratory diseases[1]. *MUC5AC* and *MUC5B* are evolutionarily conserved genes that encode structurally related mucin glycoproteins, the principal macromolecules in airway mucus[1,3]. Genetic variants are linked to diverse lung diseases[4-6], but specific roles for MUC5AC and MUC5B in MCC, and the lasting effects of their inhibition, are unknown. Here we show that Muc5b (but not Muc5ac) is required for MCC, for controlling infections in the airways and middle ear, and for maintaining immune homeostasis in the lungs. Muc5b deficiency caused materials to accumulate in upper and lower airways. This defect led to chronic infection by multiple bacterial species, including *Staphylococcus aureus*, and to inflammation that failed to resolve normally[7]. Apoptotic macrophages accumulated, phagocytosis was impaired, and IL-23 production was reduced in*Muc5b*$^{-/-}$ mice. By contrast, in *Muc5b* transgenic (Tg) mice, macrophage functions improved. Existing dogma defines mucous phenotypes in asthma and chronic obstructive pulmonary disease (COPD) as driven by increased MUC5AC, with MUC5B levels either unaffected or increased in expectorated sputum[1,8]. However, in many patients, MUC5B production at airway surfaces decreases by as much as 90%[9-11]. By distinguishing a specific role for Muc5b in MCC, and by determining its impact on bacterial infections and inflammation in mice, our results provide a refined framework for designing targeted therapies to control mucin secretion and restore MCC.

Mucosal surfaces are central interfaces between organisms and their external environments. Mucus-coated barriers defend against pathogens[12] and re-distributed commensal organisms[13]. Gastrointestinal (GI) mucins prevent *Helicobacter pylori* growth[12], colitis[14], and colorectal carcinogenesis[15]. To test whether secreted airway mucins serve correspondingly significant roles, we examined MCC and responses to bacterial infections in *Muc5ac*$^{-/-}$[16],*Muc5b*$^{-/-}$, and *Muc5b*^{Tg} mice (Extended Data Fig. 1a-d). We identified unique mechanisms by which Muc5b mediates effective respiratory mucosal defense (Extended Data Fig. 2). In *Muc5b*$^{-/-}$ upper airways, olfactory gland glycoconjugates were absent, but nasopharyngeal surfaces were unaffected (Fig. 1a, b). Muc5ac and Muc5b were lacking in respective knockout airways, but tracheobronchial glycoconjugates increased in*Muc5b*$^{-/-}$ mice due to induced Muc5ac (Fig. 1c, d, Extended Data Figs. 1f and 3). Despite retaining mucous phenotypes in many airway tissues, growth and survival were impaired in *Muc5b*$^{-/-}$ animals (Fig. 1e, f) while *Muc5ac*$^{-/-}$ and *Muc5b*^{Tg} mice survived normally (Fig. 1f). Acute MCC was normal in *Muc5ac*$^{-/-}$ and *Muc5b*^{Tg} mice, but severely reduced in *Muc5b*$^{-/-}$ mice (Fig. 1g, h and Extended Data Fig. 1e), even though functional ciliated cells were present (Fig 1d, i). Mucus transport was impaired in *Muc5b*$^{-/-}$ tracheal epithelial cells *in vitro*, confirming that defective clearance reflected altered mucociliary interactions specifically (Fig. 1j-l and Extended Data Videos 1, 2). Collectively, these data identify non-redundant protective requirements for Muc5b in survival and MCC.

Impaired MCC in *Muc5b*$^{-/-}$ mice was accompanied by abnormal breathing (Fig. 2a, b) and hypoxemia (Fig. 2c). We assessed lung function in mechanically ventilated mice. Baseline airflow and responses to the bronchoconstricting agent methacholine were normal in the

lower airways (Fig. 2d-f). Circumventing the upper airways restored ventilation in spontaneously breathing tracheostomized animals (Fig. 2g, Extended Data Videos 3, 4). Thus, upper respiratory obstruction impeded airflow in *Muc5b*$^{-/-}$ mice. Micro-CT confirmed this with radiological evidence of upper airway obstruction (Fig 2h), and middle ear effusion consistent with otitis media (OM) (Extended Data Fig. 4a, b). The latter was unexpected given associations between increased MUC5B and human OM[17]. In *Muc5b*$^{-/-}$ mice, but not *Muc5ac*$^{-/-}$ mice (data not shown), hair fragments encased in mucus-like material were consistently found in posterior nasopharynxes (Fig. 2i, j, Extended Data Fig. 4c) and middle ears (Fig. 3a and Extended Data Fig. 4d). Bacteria and inflammation in *Muc5b*$^{-/-}$ middle ear lavage samples confirmed infectious OM (Fig. 3b, c).

In *Muc5b*$^{-/-}$ lower airways, aspirated materials and inflammatory infiltrates were also common (Fig. 3d, e). Culturable bacteria in the lungs increased 2.9-21.6 fold over time, and 7.6-75 fold further in spontaneously moribund mice who also had increased bacteria in spleen cultures (Fig. 3f, g), suggesting that disseminated infections contributed to mortality. To test this hypothesis, mice were placed on antibiotic-supplemented diets. Antibiotics reversed spontaneous lethality and reduced lung bacterial burden, but did not restore normal ventilation in *Muc5b*$^{-/-}$ mice (Fig. 3h-j). Thus, the cause of death in *Muc5b*$^{-/-}$ mice was infectious, and not directly due to airflow limitation. These data identify a natural course in which *Muc5b* deficiency causes upper airway obstruction, spontaneous infection of connecting auditory tubes and the lungs, and fatal bacteremia.

Because of the importance of bacterial infection in *Muc5b*$^{-/-}$ mice, we identified organisms whose accumulation in the lungs was normally prevented by Muc5b-rich mucus. 16S rRNA phylotyping revealed 19 genera and >25 species in the lungs. Most were oral, gut, and skin microbiota. At 3 mos age, populations were heterogeneous and indistinguishable (Fig. 3k and Extended Data Fig. 5). However, in moribund *Muc5b*$^{-/-}$ lungs, streptococci and staphylococci increased significantly (Fig. 3k). One streptococcal species, (*S. acidominimus*) increased in abundance but was also frequently found in controls (Extended Data Fig. 5f-h). By contrast, *Staphylococcus aureus*, an important pneumonia-causing pathogen, selectively increased in spontaneously moribund *Muc5b*$^{-/-}$ mice (150-389 fold; Fig. 3k). Its incidence was 78% in moribund mice compared to 25% in 3 mo old *Muc5b*$^{-/-}$ mice, and 8% in *Muc5b*$^{+/+}$ mice (χ^2p=0.002). Moribund mouse spleen cultures contained bacteria also found in the lungs, including *S. aureus* (Extended Data Fig. 6). Based on these associations, we tested the effects of mucin expression on pathogenesis following airway inoculation with *S. aureus* USA300[18]. Though non-lethal in *Muc5b*$^{+/+}$, *Muc5b*^{Tg}, and *Muc5ac*$^{-/-}$ animals, only 40% of *Muc5b*$^{-/-}$ mice survived (Fig. 3l, Extended Data Fig. 7a-e). Thus, Muc5b is selectively required for preventing acquisition and enrichment of virulent bacteria such as *S. aureus* in the airways.

The airways are exposed to bacteria from birth onward. MCC is considered the major route for their elimination. However, although *Muc5b*$^{-/-}$ mice showed severely impaired MCC, most survived several months with increased lung bacterial burden (Figs. 1f and 3f, h), but were ultimately unable to control *S. aureus* infection (Fig. 3k, l). Therefore, we investigated additional potential mechanisms forMuc5b-dependent airway defense. Purified MUC6 (but not MUC5AC) inhibits *H. pylori* growth[12], and purified MUC5AC (but not MUC2) inhibits

Trichuris muris survival[16]. However, neither MUC5AC nor MUC5B inhibited *S. aureus* growth (Extended Data Fig. 7f), suggesting that Muc5b-mediated defense was not mediated by direct inhibitory interactions with *S. aureus*.

We then investigated whether *Muc5b* deficiency affected inflammatory defenses. Leukocytes in *Muc5b*$^{-/-}$ lung lavage fluid were significantly altered. In the steady state, neutrophils and eosinophils accumulated, but lymphocytes were absent (Extended Data Fig. 8a). There were also striking changes in macrophages in *Muc5b*$^{-/-}$ lungs. Macrophages accumulated over time (Fig. 4a). They frequently contained undigested cytoplasmic inclusions (Fig. 4b), and had impaired phagocytic functions (Extended Data Fig. 9a). By age 12 mos., IL-23, a mediator of anti-microbial inflammatory responses normally produced by macrophages and dendritic cells, was reduced by 93% in *Muc5b*$^{-/-}$ mice (Fig. 4c, Extended Data Table 1). As *Muc5b*$^{-/-}$ mice became moribund over this timecourse, dysfunctional inflammatory phenotypes progressed (Fig. 4d, Extended Data Fig. 8a). Macrophages that accumulated in airspaces were increasingly apoptotic (Fig. 4e, f). IL-23 remained significantly lower in moribund *Muc5b*$^{-/-}$ mice than controls (Fig. 4g), despite their severely infected states (Fig. 3f, k). We found no evidence that macrophages produce Muc5b (Extended Data Fig. 9b), so it is unlikely that these pathologies were cell autonomous. Rather, the ability of *Muc5b*$^{-/-}$ lungs to resolve inflammation following microbial exposure was significantly inhibited[7].

Apoptotic macrophage accumulation in *Muc5b*$^{-/-}$ mice suggests that in addition to acute microbial elimination, MCC is required for chronically maintaining phagocyte clearance and immune functions *in vivo*. We thus tested the impacts of age and Muc5b expression on acute and resolving lung inflammation following *S. aureus* infection. In young animals, acute neutrophilic responses were similar irrespective of genotype (Extended Data Fig. 8b). By contrast, aged *Muc5b*$^{-/-}$ animals were exquisitely sensitive, exhibiting 100% mortality within the first few hours of infection, while *Muc5b*$^{+/+}$ and *Muc5b*^{Tg} mice survived (Fig. 4h). Thus, the combined absence of MCC and the chronic effects of underlying spontaneous infections enhanced the deleterious consequences of *S. aureus* infection. Young mice survived to day 7 post-infection, a peak timepoint of resolving inflammation[7]. Infected *Muc5b*$^{-/-}$ lungs exhibited increases in lung macrophages and mixed granulocytes (Fig. 4h and Extended Data Fig. 8c). Accumulated macrophage pools were predominated by apoptotic cells (Fig. 4i) and linked to significantly reduced lung IL-23 (Fig. 4j), similar to spontaneously moribund *Muc5b*$^{-/-}$ mice. Conversely, in *Muc5b*^{Tg} mice, IL-23 production, macrophage activation, and *S. aureus* elimination were enhanced (Fig. 4j-l).

Collectively, these data show that Muc5b expression affects inflammation and macrophage-mediated responses in the lungs. In its absence, mice failed to mount effective anti-bacterial responses. In its sustained presence, these were enhanced. Apoptotic cells, including neutrophils, accumulated in MCC deficient *Muc5b*$^{-/-}$ airspaces (Fig. 4e, Extended Data Fig. 9c). Efferocytosis of neutrophils is reported to down-regulate IL-23[19], which may explain its decline in the lungs. It will be of great interest to test the degrees to which Muc5b-dependent changes in macrophages are mediated by altered elimination due to impaired MCC, and by other processes such as opsonization or pharmacologic interactions[20]. Nonetheless, these studies functionally link two fundamental first line host defense components – mucus and

phagocytes. To the best of our knowledge, Muc5b is the only bronchial secretory protein identified to date demonstrating such singularly strong biological necessity. Mice survive normally in the absence of Muc5ac or anti-microbial peptides such as βdefensin-1[21], calgranulin B[22], lipocalin-2[23], or lactoferrin[24]. In addition to controlling MCC and macrophage readiness, it is conceivable that Muc5b is a scaffold for these and other defensive molecules.

The novel relationships between Muc5b, MCC, and inflammation reported here have the potential to impact therapies for airway diseases. Cystic fibrosis, COPD, and asthma are associated with mucus hypersecretion, impaired MCC, and increased risk for respiratory infections[25-29]. *MUC5AC* and *MUC5B* expression varies among individuals, but the overall result is excessive mucin production[1,8-11]. Such pathological associations have overshadowed the benefits of airway mucus and the potential functions of individual mucins in infections[1,12,13,15,16,30]. Human *MUC5B* is highly polymorphic. A recently identified promoter variant found in ~20% of the general population increases its expression 37.4-fold in healthy lungs[5]. Our findings in *Muc5b* deficient and overexpressing mice suggest that *MUC5B* variants may regulate airway homeostasis, disease pathogenesis, and mucosal immune function in humans broadly. While controlling mucin hypersecretion is an attractive therapeutic goal for transient and chronic lung diseases[1], a therapy that completely disrupts mucus and inhibits MUC5B for extended periods may not be advisable. Rather, promoting adequate expression and enhancing MCC and airway defense in controlled manners are better strategies.

Methods Summary

Mice were used with Institutional Animal Care and Use Committee approvals. *Muc5ac*$^{-/-}$ mice were generated previously[16]. *Muc5b*$^{-/-}$ and *Muc5b*^{Tg} mice were generated here. Muc5b protein was assessed immunohistochemically using rabbit polyclonal antisera. Ciliary beat, MCC, and transport were assessed as described previously. Lung function was measured using a head-out plethysmograph and a flexiVent (Scireq, Montreal, Quebec, Canada), and blood oxygen was assessed using a pulse oximeter. Otitis media was assessed by visual otoscopy and middle ear lavage (MEL). Pulmonary inflammation was assessed by histology and lung lavage. Lavaged leukocytes were identified by light microscopy and flow cytometry. Neutrophils, macrophages, MHC-II, and apoptotic cells, were detected using commercially available Ab'S and reagents. *S. aureus* was administered by 10 μl intranasal or 50 μl intratracheal inocula at 10^7-10^8 CFU/animal. Bacteria and bacterial DNA were isolated from MEL, lung homogenates, and lung lavage pellets. Isolated colonies were phylotyped by 16S rRNA and *mecA* sequencing. Kaplan-Meier (**1f** and **3h**, **l**), regression (**1e** and **2f**), one-sided t-test (**1g-i**, **k**, **l**; **2b-e**, **g**; **3b**, **c**, **f**, **g**, **j**, **k**, and **4c**, **d**, **f**, **g**, **i**, **j**), and one-way ANOVA (**3i** and **4a**, **h**, **j**, **l**) with appropriate corrections for multiple comparisons, unequal variances, and non-Gaussian distribution were carried out using GraphPad Prism v5.04 (GraphPad Software, Inc., La Jolla, CA). Full methods are found in Supplementary Information.

Methods

Mouse husbandry

Male and female specific pathogen free, 6-8 week old C57BL/6J mice were purchased from the Jackson Laboratory (Bar Harbor, ME). Mice were housed in accordance with the Institutional Animal Care and Use Committees of the MD Anderson Cancer Center, the University of Colorado School of Medicine, and the University of North Carolina-Chapel Hill. Mice were kept in specific pathogen free housing areas that were maintained by institutional animal care staff. Mice were fed *ad libitum* either a normal diet of water and irradiated chow (Harlan Teklad, Indianapolis, IN), or in specified experiments, the same diet supplemented with trimethoprim and sulfadiazine (275 and 1,365 mg/kg chow, respectively) and enrofloxacin (2.7 mg/ml drinking water). Mice used for survival analysis were assigned prior to genotype identification and were studied up to 12 months age. Moribund mice were identified by observing changes in body weight and behaviors. In accordance with the veterinary care procedures at MD Anderson and UC Denver, a loss of >15% of body weight without recovery, hunching, fur ruffling, and lethargy were used as criteria for determining moribundity. For all other studies, mice were assigned non-descriptive numbers at weaning. Aside from knowledge of a particular strain background, genotypes were unknown during experiments and post-experimental analyses. These criteria held during inflammation, microscopy, and bacterial species identification studies, which were performed by different investigators. Male and female mice were used in all studies. Animals were euthanized by exsanguination under anesthesia or asphyxiation by CO_2 inhalation.

Genetically engineered mice

Muc5ac knockout mice were generated previously[16]. *Muc5b* knockout mice were generated using a targeting allele with LoxP sites flanking exon 1 (fig S1). The targeting allele was linearized with NotI and electroporated into CJ7 embryonic stem cells at the MD Anderson Cancer Center Genetically Engineered Mouse Facility. Homologous insertion of the targeting allele was confirmed by long-range PCR, restriction digest, and DNA sequencing (fig S1). One targeting allele-positive cell line was expanded and inserted into albino C57BL/6J blastocysts to generate chimeric founders. CJ7 cells are derived from a 129S1 mouse with an agouti coat color. Chimeric males were mated with C57BL/6J females, and agouti progeny were screened for targeting allele transmission. Positive mice were subsequently bred with Rosa26-Flpe recombinase knock-in animals to remove the neomycin selection cassette. Progeny were crossed with CMV-Cre transgenic mice to generate full knockout animals, resulting in animals that were heterozygous mosaics for *Muc5b* ($Muc5b^{\Delta/-}$) in all tissues, including the germline. Germline transmission was confirmed by breeding Cre positive $Muc5b^{\Delta/-}$ and wild type C57BL/6J mice. *Muc5b* recombinant progeny were thus identified as $Muc5b^{\Delta/+}$. F1 $Muc5b^{+/-}$ mice were intercrossed, and resulting litters were viable with typical Mendelian inheritance distributions. Mice were continuously backcrossed by breeding heterozygotes with wild type C56BL/6J mice for >5 generations using strain-specific microsatellite marker facilitated analysis (speed congenics) to confirm congenic status (>99%). For the studies reported here, *Muc5b* and *Muc5ac* targeted mice were maintained by heterozygous crossing using littermates for comparisons.

Muc5b transgenic mice were generated by insertion of the full length 34 kb genomic coding region of the mouse *Muc5b* gene into a rat Scgb1a1 promoter-IRES-AcGFP transgenic targeting cassette using recombinegenic cloning[31]. Founders were generated by injecting the targeting vector into C57BL/6N pronuclei at the National Jewish Health transgenic mouse core. Due to the size of the DNA, only 2 lines of fertile mice were made. One line demonstrated significant overproduction of Muc5b protein by Western blot, and all signals were >1 MDa on agarose gels, indicating that both native and transgenic Muc5b were extensively glycosylated. Expression was also examined immunohistochemically, and extensive expression throughout the lungs was found (Extended Data Fig. 1). These mice were maintained by continuous hemizygous outcrosses with C57BL/6J mice.

Immunohistochemistry

Loss of expression of *Muc5b* was confirmed immunohistochemically using rabbit-anti-mouse Muc5b antisera as described previously[32,33]. The peptide used to generate this antisera is repeated 5 times in the full length protein, and the DNA regions encoding it are >20-25 kb 3' to the excised region in *Muc5b*$^{-/-}$ mice. Tissues from wild type mice demonstrated expression in the nasal turbinates, tracheal submucosal glands, and throughout the bronchial tree (see Fig. 1). No signal was detected in tissues from knockout mice, thus indicating that disruption of exon 1 was sufficient to abolish Muc5b protein production.

To detect cytospun neutrophils, macrophages, and apoptotic cells, NIMP-R14 (1:500, Abcam, Cambridge, MA) followed by Alexa-594 conjugated anti-rat IgG (Life Technologies, Carlsbad, CA), FITC conjugated F4/80 (1:100, BM8, eBioscience, San Diego, CA), and polyclonal anti-activated caspase 3 (1:500, ab13847, Abcam) followed by Alexa-647 conjugated anti-rabbit IgG (Life Technologies) were used, respectively. NIMP-R14 was also used to individually assess neutrophil accumulation in tissue sections using HRP-conjugated secondary antisera followed by DAB for detection. Antibodies were diluted in 0.01% Tween 20 diluted in PBS. Hoechst 33342 or hematoxylin was used to counterstain nuclei. Cells and tissues were imaged on an upright Olympus BX60 or BX63 microscope and imaged using Olympus DP70 and DP72 cameras (Olympus America, Center Valley, PA). Subsequent analysis of colocalization in fluorescent stained cells was made using cellSens digital imaging software (Olympus). Isotype control antibodies were used to confirm specificity of immunolabeling experiments.

Mucociliary clearance in vivo

Tracheal ciliary beat frequency was measured as described previously[34]. Mucociliary clearance was measured by assessing the elimination of fluorescent microspheres from the nose as described previously[35] and from the lungs using a method adapted from Coote *et al*[36]. For pulmonary clearance 5×10^5 yellow-green fluorescent carboxylate-modified microspheres (Fluospheres, Life Technologies, Carlsbad, CA) were instilled intratracheally using a Penn-Century microsprayer via a transoral route in urethane anesthetized mice (2 g/kg, ip). Mice were euthanized by exsanguination immediately or 15 min after Fluosphere administration. Lungs and trachea (up to but not including the larynx) were excised, placed in vials containing PBS/0.1% Tween 20 and 1 mm diameter glass beads, and homogenized by agitating at 4,800 oscillations/min for 10 s using a Mini-Beadbeater-1 (Bio-Spec

Products, Bartlesville, OK). Homogenized material was placed on a hemacytometer, and beads remaining in the lungs were quantitated under epifluorescence on an Olympus BX60 microscope (Olympus America, Inc., Center Valley, PA). Baseline deposition was assessed by averaging the numbers of Fluospheres detected in the lungs in mice euthanized immediately after installation. Out of 5×10^5 beads administered, means ± sem's of $3.98 \pm 0.50 \times 10^5$ beads were observed in *Muc5b*$^{+/+}$ animals, and $3.66 \pm 0.4.3 \times 10^5$ beads were observed in *Muc5b*$^{-/-}$ animals at time zero (79.6% and 73.2% deposition fractions, respectively). These baseline values were not significantly different (t-test p-value = 0.64). Numbers of beads remaining in mice euthanized 15 min after installation were then measured. Fractional clearance was calculated by subtracting the ratio of the numbers of beads remaining in the lungs at 15 min over the average at time zero for each genotype (n = 8-11 for time zero data). This ratio was subtracted from 1 and the difference was multiplied by 100 to calculate percent clearance.

Mucociliary transport in vitro

Mucociliary transport was measured *in vitro* by culturing mouse tracheal epithelial cells (mTEC's) as described previously[37,38]. For these studies cultures were grown on collagen coated 4.67 cm^2 transwell inserts in 6 well plates. Five tracheas were used to derive epithelial cells to seed each well at a density of 5×10^5 cells/well. Confluent cultures were transitioned to air-liquid interface and maintained for an additional 21-28 days. Mucociliary transport was assessed by adapting methods previously used in human airway epithelial cell cultures[39]. Briefly, red carboxylate-modified Fluospheres (4 μm diameter) were diluted to a concentration of 2×10^3/μl in 300 mOsm mannitol[40]. These were added to the centers of transwells in a volume of 5 μl and placed in a 37°C incubator for 30 min to allow bead dispersion and airway surface liquid normalization. Wells were observed on an Olympus IX-81 inverted microscope under red fluorescence. Time lapse images were acquired at 30 s intervals under 10 × magnification for 15 min and were analyzed using Slidebook 4.0 software (Olympus). Transport distance and displacement measured for all particles in two separate mTEC cultures from 10 *Muc5b*$^{+/+}$ and 10 *Muc5b*$^{-/-}$ mice. Values were calculated for 124 Fluospheres in *Muc5b*$^{+/+}$ and 95 Fluospheres *Muc5b*$^{-/-}$ cultures, respectively. Data were analyzed for particles that traveled a distance greater of than 4 μm (the diameter of a single bead) to exclude effects of vibration and Brownian motion.

Mouse physiology

Ventilation was measured in conscious mice using a head out plethysmograph (Scireq, Montreal, Canada). Tidal volume, respiratory rate, and minute ventilation were measured for each animal. Mice were restrained in chambers separated with a custom fit neck seal made of 0.02" thick silicone rubber (35A durometer rating; McMaster-Carr, Robbinsville, NJ). Plethysmography was assessed in real time and recordings were made after a 2-5 min acclimation period. Data were averaged over 5-10 min periods in which resting breath patterns were observed.

Arterial blood oxygen saturation was assessed in mice using a MouseOx mouse pulse oximeter (STARR Life Sciences Corp, Oakmont, PA). For studies in conscious mice, fur around the neck was removed with clippers in order to use a collar clip LED sensor. Percent

oxygen saturation (SaO_2) of functional arterial hemoglobin was measured in room air and in the presence of 100% O_2 (fraction of inspired oxygen, FiO_2 = 1.0). Data were analyzed from n = 4 *Muc5b*$^{+/+}$ and n = 5 *Muc5b*$^{-/-}$ mice. For arterial oxygen saturation measurements pre and post tracheostomy, mice were anesthetized by inhalation of ~2% isoflurane in room air and SaO_2 was measured with the MouseOX using a thigh clip. When a stable reading was obtained, the anesthetized mouse was tracheostomized by exposing the trachea and cutting a ~1 mm opening with micro scissors just below the larynx, through which the mouse breathed. The SaO_2 was again measured following the tracheostomy. Despite their chronic hypoxemic states, which would be expected to increase hematocrit, *Muc5b*$^{-/-}$ mice had slightly reduced circulating red blood cell numbers compared to *Muc5b*$^{+/+}$ littermates (~7% decrease), consistent with the development of anemia of chronic disease[41-43].

Pulmonary function was analyzed using a flexiVent (Scireq, Montreal, Canada). Mice were anesthetized with urethane (2.0 g/kg, i.p.). This dose is sufficient to provide 6-8 h of sedation, though experiments lasted only 20-30 min. Mice were tracheostomized with a blunt beveled 18 G Luer stub adapter, and once ventilated (150 breaths/min, 10 ml/kg, against 3 cmH2O positive end expiratory pressure - PEEP), they were paralyzed by continuous infusion of succinylcholine chloride (10 mg/kg/min, i.p.). Total lung resistance (R_L) and airway resistance (R_{aw}) were assessed at baseline and in response to successive increasing methacholine (MCh) doses (0.1, 0.3, 1, 3, and 10 mg/ml) administered by an in-line ultrasonic nebulizer. At the highest dose of MCh (10 mg/ml) heart rates assessed by electrocardiogram often fell below 100 bpm and did not recover. At this point, no further doses responses were performed.

Micro-CT imaging

Mice were anesthetized with isoflurane, positioned on a warming bed and the head imaged with a GE eXplore CT120 scanner, 70 kV, 50 mA, 100 μm isotropic scans. All mice recovered uneventfully from this procedure.

Examination of middle ear inflammation and infection

To visualize the ear drum *in vivo*, the mouse was anesthetized with isoflurane and positioned under a dissecting microscope. An “otoscope” was fashioned using a pipette tip, the large end of which was interfaced with a fiberoptic light. The small end of the pipette tip, cut to a diameter of ~1 mm, was inserted into the external auditory ear canal. Using this procedure the ear drum was visualized and photographed.

For middle ear lavage (MEL), mice were euthanized by exsanguination under anesthesia. The mandible was removed. Tympanic bullae were exposed by blunt dissection and thoroughly wiped with sterile cotton swabs and betadine to sterilize the external surface. A small incision was made on the ventral side of the tympanic bulla using a 23G needle and a blunt 30G needle was inserted. Middle ear lavage was performed by instilling and retrieving 2 × 10 μl of sterile PBS. MEL total cells were counted with a hemocytometer, cytospin slides were obtained (StatSpin Cytofuge 2, Norwood, MA), air dried, and stained with modified Giemsa (NewComer Middleton, WI) for differential cell counts of at least 200 cells per slide.

Bacterial, isolation, growth and sequencing

Bacteria were cultured from lungs of mice homogenized as described above for Fluosphere isolation. Aliquots of homogenates of MEL lavage cells were serially diluted and grown on tryptic soy agar plates as described previously[44] in humidified 37°C incubators under atmospheric oxygen, under nitrogen charged hypoxic (<1% O_2) conditions and in the presence of 5% CO_2, or in a candle jar on Columbia anaerobe sheep blood agar (Becton Dickinson, NJ). Plates were incubated at 37°C for 24 h, and colony forming units (CFU) were enumerated. Colonies were counted 18-24 h after incubation. Ten colonies were picked at random from each sample and grown in 2 ml tryptic soy broth under the aerobic/anaerobic conditions above, except when <10 colonies were present, in which case all colonies were picked and grown. Expanded cultures were pelleted and DNA was isolated using Fast DNA Spin kits (MP Bio, Solon, OH). Ribosomal 16S sequencing was conducted in a 25 μl volume with 2 μl bacterial DNA (Bioline MyTaq™ HS Red Mix), using forward primer 27F 5'-AGAGTTTGATCMTGGCTCAG and reverse primer 1492R 5'-TACGGYTACCTTGTTACGACTT (at 0.4 pM; where M = A or C; Y = C or T). Cycling conditions were 95°C for 5 min followed by 35 cycles of 95°C for 30 sec, 58°C for 30 sec, and 72°C for 30 sec, followed by one 7 min extension at 72°C. PCR products were purified using ExoSAP-IT (Affymetrix, Santa Clara, CA). Samples were prepared for sequencing (GENEWIZ, Inc., South Plainfield, NJ) by mixing 10μL of each PCR product with 5 μL of the sequencing primer 5'-CCGTCAATTCCTTTRAGTTT. Sequences were aligned using nucleotide BLAST (http://blast.ncbi.nlm.nih.gov/), microbial genomic BLAST (http://www.ncbi.nlm.nih.gov/sutils/genom_table.cgi?organism=microb), Ribosomal Database Project (http://rdp.cme.msu.edu/), and Greengenes http://greengenes.lbl.gov/cgi-bin/nph-index.cgi[45] search tools. Microbial genera were identified in cases in which results demonstrated >97% sequence similarities, and species were identified in cases where sequence similarities were >99%[46]. To confirm findings in some cases, sequencing of the RNase P *rnpB* gene was amplified using the strF 5'-YGTGCAATTTTTGGATAAT and strR 5'-TTCTATAAGCCATGTTTTGT 3' primers, and products were sequenced and analyzed as described above. For *Staphylococcus aureus* pneumonia experiments, bacteria were grown as described previously and administered by 10 μl intranasal inoculations or 50 μl intratracheal bolus challenges[18].

Leukocyte identification and functional analysis

Blood was obtained by cardiac puncture in order to measure hematocrit and circulating leukocytes. No differences were seen in hematocrit in *Muc5b*$^{-/-}$ mice compared to *Muc5b*$^{+/+}$ littermates at 12 weeks of age. There was a small increase in circulating leukocyte numbers in *Muc5b*$^{-/-}$ mice compared to *Muc5b*$^{+/+}$ mice (7.53 ± 1.62 vs. 5.12 ± 0.12 × 10^3μl), but these differences were not statistically significant. To assess lung leukocytes, the lungs were lavaged using 2 × 1 ml PBS introduced via a 20 G tracheal cannula. Cells were counted on a hemacytometer. Samples were centrifuged (300 × g, 5 min), supernatants were stored in liquid N_2, and pellets were resuspended in 1 ml PBS. To identify leukocytes in lavage fluid, cells were cytospun and stained with Wright-Giemsa. In a small number of wild type C57BL/6J mice, an aerosolized lysate of a clinical isolate of Non-typeable *Haemophilus influenzae* (NTHi) was administered to induce inflammation and

cytokine production for use as positive controls in the current studies[47]. In some cases, cells stained with anti-macrophage (F4/80 clone BM8, eBioscience, San Diego, CA) and anti-neutrophil (NIMP-R14, Abcam, Cambridge, MA) markers were used to confirm differential identification. NIMP-R14 recognizes Ly6G and Ly6C antigens (like GR1, see below). NIMP-R14 specificity was tested in lavage from NTHi exposed mice 24 h post exposure. Following NTHi, neutrophils had high fluorescence intensity and typical polymorphonuclear appearances, while macrophages were negative. Staining in *Muc5b*$^{-/-}$ lavage samples was performed simultaneously, and image acquisition settings were identical to those used in wild type NTHi exposed samples.

For flow cytometry, mice were lavaged with 5 × 1 ml PBS with 1mM EDTA. Cell suspensions were incubated with Fc blocking antibodies for 20 minutes and then incubated with fluorochrome-conjugated monoclonal antibodies for 30 minutes. Cell were washed twice, fixed with 1% paraformaldehyde and assayed using a BD LSR-II flow cytometer. Data were analyzed with FloJo Software (Tree Star, Ashland, OR). Cells were identified with forward and side scatter and doublets were excluded. Alveolar macrophages were identified with F4/80 (6F12) and CD11c (HL3). Neutrophils were defined as GR1^{high} CD11b^{high} F4/80^{neg} CD11c^{neg} events. Macrophage activation was assessed with monoclonal antibodies directed at MHCII (In-1), CD86 (GL1) and CD40 (3/23). All antibodies were obtained from BD Biosciences (Franklin Lakes, NJ). Lavage supernatants were analyzed for cytokine production by a commercial service (Aushon Biosystems, Billerica, MA; Extended Data Table 1), and IL-23 was confirmed by ELISA (eBioscience, cat no. BMS6017).

Leukocyte phagocytosis was assessed in separate animals using a method adapted from Steinkamp *et al*.[48]. Lavage fluid was collected from 12 week old animals as described above, with the exception that RPMI 1640 medium (Life Technologies, Carlsbad, CA) was used for lavage instead of PBS. Lavage volume was normalized to 1.75 ml with RPMI, and 250 μl of PBS containing 10^7 2 μm diameter yellow-green Fluospheres was added to each lavage sample and incubated for 30 min in a 37°C shaking incubator under gentle agitation (50 rpm). Samples were then placed on ice for 1-2 min, centrifuged for 10 min at 4° C at 300 × g, washed in 1 ml PBS, and recentrifuged for 10 min at 4°C at 300 × g. The pellet was then resuspended in a 200 μl solution of 10 μg/ml Hoechst 33342 in PBS. Cells were imaged and counted on a hemacytometer under epifluorescence as described above. Due to the presence of an efflux pump in macrophages, 88% of Fluosphere positive cells were Hoechst dye low or negative.

To detect total bacteria and methicillin resistant *S. aureus* 7 d post-infection, lung lavage cell pellets were analyzed by quantitative PCR as described previously[49]. Total DNA was isolated from pellets using a MO-BIO Soil DNA purification kit, per the manufacturer's directions. *16S rRNA* gene DNA was amplified as described[21]. To identify the presence of the methicillin resistant *S. aureus* strain used here, a separate SYBR green qPCR detection strategy was employed to quantify *mecA* gene copy number using the following primers: sense 5'-GATGGTATGTGGAAGTTAGATTGG-3'; antisense 5'-CGGTTTTAAGTGGAACGAAGG-3'). Amplified *mecA* copy number was normalized to lavage volume and *16S rRNA* gene content. Standard curves were generated using purified

PCR products, and water was used as a negative control. 16S PCR was sensitive to a lower detection limit of 100 copies, and *mecA* was sensitive to a single copy.

Statistical analyses

All analyses were carried out using GraphPad Prism v5.04 (GraphPad Software, Inc., La Jolla, CA). Numbers of mice used to detect changes in survival were based upon prior studies from our lab using models of infectious pneumonia and cancer[44,50]. All other studies were based upon prior experience using inflammation, infectious pneumonia, mucous clearance, and lung function from our labs[36,51]. Means and variances from prior findings in wild type mice served as the basis to determine sample sizes required to detect significant differences at 0.80 power.

Supplementary Material

Refer to Web version on PubMed Central for supplementary material.

Acknowledgments

We thank F. Ttofali, D. Harper, D. Raclawska, V. Mdoe, C. Ramsey, and J. Parker-Thornburg for their assistance. We also thank K. Naff and the MD Anderson Cancer Center Department of Veterinary Medicine and Surgery for excellent support in animal care. This work was supported by the National Institutes of Health Grants R01 HL080396 (C.M.E.); R01 AA008769 (J.H.S.), R01 HL109517 (W.J.J.); R01 HL114381 (P.M.H.); R01 HL097000 (B.F.D.), P01 HL108808, P01 HL110873, P50 HL107168, P30 DK065988 (R.C.B.) and Cystic Fibrosis Foundation Grants 06IO (C.M.E.) and RDP R026-CR11 (R.C.B.). Additional support was provided by National Institutes of Health Cancer Center Support Grant CA016672 for the MD Anderson Cancer Center Genetically Engineered Mouse facility; by CA016086 for the UNC Biomedical Research Imaging Center Small Animal Imaging Facility, and for the UNC Michael Hooker Microscopy Facility funded by an anonymous private donor.

References and notes

1. Fahy JV, Dickey BF. Airway mucus function and dysfunction. New England Journal of Medicine. 2010; 363:2233–2247. [PubMed: 21121836]
2. Button B, et al. A periciliary brush promotes the lung health by separating the mucus layer from airway epithelia. Science. 2012; 337:937–941. doi:10.1126/science.1223012. [PubMed: 22923574]
3. Young HW, et al. Central role of muc5ac expression in mucous metaplasia and its regulation by conserved 5' elements. Am J Respir Cell Mol Biol. 2007; 37:273–290. [PubMed: 17463395]
4. The Collaborative Study on the Genetics of, A. A genome-wide search for asthma susceptibility loci in ethnically diverse populations. Nature Genetics. 1997; 15:389–395. [PubMed: 9090385]
5. Seibold MA, et al. A common muc5b promoter polymorphism and pulmonary fibrosis. N Engl J Med. 2011; 364:1503–1512. doi:10.1056/NEJMoa1013660. [PubMed: 21506741]
6. Kamio K, et al. Promoter analysis and aberrant expression of the muc5b gene in diffuse panbronchiolitis. Am J Respir Crit Care Med. 2005; 171:949–957. [PubMed: 15709052]
7. Janssen WJ, et al. Fas determines differential fates of resident and recruited macrophages during resolution of acute lung injury. Am J Respir Crit Care Med. 2011; 184:547–560. doi:10.1164/rccm.201011-1891OC. [PubMed: 21471090]
8. Thornton DJ, Rousseau K, McGuckin MA. Structure and function of the polymeric mucins in airways mucus. Annu.Rev.Physiol. 2008; 70:459–486. [PubMed: 17850213]
9. Woodruff PG, et al. T-helper type 2-driven inflammation defines major subphenotypes of asthma. Am J Respir Crit Care Med. 2009; 180:388–395. doi:10.1164/rccm.200903-0392OC. [PubMed: 19483109]
10. Innes AL, et al. Epithelial mucin stores are increased in the large airways of smokers with airflow obstruction. Chest. 2006; 130:1102–1108. [PubMed: 17035444]

11. Ordonez CL, et al. Mild and moderate asthma is associated with airway goblet cell hyperplasia and abnormalities in mucin gene expression. Am J Respir Crit Care Med. 2001; 163:517–523. doi: 10.1164/ajrccm.163.2.2004039. [PubMed: 11179133]
12. Kawakubo M, et al. Natural antibiotic function of a human gastric mucin against helicobacter pylori infection. Science. 2004; 305:1003–1006. [PubMed: 15310903]
13. Johansson ME, et al. The inner of the two muc2 mucin-dependent mucus layers in colon is devoid of bacteria. Proc.Natl.Acad.Sci.U.S.A. 2008; 105:15064–15069. [PubMed: 18806221]
14. van der Sluis M, et al. Muc2-deficient mice spontaneously develop colitis, indicating that muc2 is critical for colonic protection. Gastroenterology. 2006; 131:117–129. [PubMed: 16831596]
15. Velcich A, et al. Colorectal cancer in mice genetically deficient in the mucin muc2. Science. 2002; 295:1726–1729. [PubMed: 11872843]
16. Hasnain SZ, et al. Muc5ac: A critical component mediating the rejection of enteric nematodes. J Exp Med. 2011; 208:893–900. doi:10.1084/jem.20102057. [PubMed: 21502330]
17. Preciado D, et al. Muc5b is the predominant mucin glycoprotein in chronic otitis media fluid. Pediatr Res. 2010; 68:231–236. doi:10.1203/00006450-201011001-00451 10.1203/PDR. 0b013e3181eb2ecc. [PubMed: 20531251]
18. Labandeira-Rey M, et al. Staphylococcus aureus panton-valentine leukocidin causes necrotizing pneumonia. Science. 2007; 315:1130–1133. doi:10.1126/science.1137165. [PubMed: 17234914]
19. Stark MA, et al. Phagocytosis of apoptotic neutrophils regulates granulopoiesis via il-23 and il-17. Immunity. 2005; 22:285–294. [PubMed: 15780986]
20. Patnode ML, et al. Galactose-6-o-sulfotransferases are not required for the generation of siglec-f ligands in leukocytes or lung tissue. J Biol Chem. 2013 doi:10.1074/jbc.M113.485409.
21. Moser C, et al. Beta-defensin 1 contributes to pulmonary innate immunity in mice. Infect Immun. 2002; 70:3068–3072. [PubMed: 12010999]
22. Manitz MP, et al. Loss of s100a9 (mrp14) results in reduced interleukin-8-induced cd11b surface expression, a polarized microfilament system, and diminished responsiveness to chemoattractants in vitro. Mol Cell Biol. 2003; 23:1034–1043. [PubMed: 12529407]
23. Flo TH, et al. Lipocalin 2 mediates an innate immune response to bacterial infection by sequestrating iron. Nature. 2004; 432:917–921. doi:10.1038/nature03104. [PubMed: 15531878]
24. Ward PP, Mendoza-Meneses M, Cunningham GA, Conneely OM. Iron status in mice carrying a targeted disruption of lactoferrin. Mol Cell Biol. 2003; 23:178–185. [PubMed: 12482971]
25. O'Riordan TG, Zwang J, Smaldone GC. Mucociliary clearance in adult asthma. Am Rev Respir Dis. 1992; 146:598–603. doi:10.1164/ajrccm/146.3.598. [PubMed: 1519834]
26. Goodman RM, Yergin BM, Landa JF, Golivanux MH, Sackner MA. Relationship of smoking history and pulmonary function tests to tracheal mucous velocity in nonsmokers, young smokers, ex-smokers, and patients with chronic bronchitis. Am Rev Respir Dis. 1978; 117:205–214. [PubMed: 637405]
27. Rowe SM, Miller S, Sorscher EJ. Cystic fibrosis. N Engl J Med. 2005; 352:1992–2001. doi: 10.1056/NEJMra043184. [PubMed: 15888700]
28. Talbot TR, et al. Asthma as a risk factor for invasive pneumococcal disease. N Engl J Med. 2005; 352:2082–2090. doi:10.1056/NEJMoa044113. [PubMed: 15901861]
29. Lee TA, Weaver FM, Weiss KB. Impact of pneumococcal vaccination on pneumonia rates in patients with copd and asthma. J Gen Intern Med. 2007; 22:62–67. doi:10.1007/ s11606-007-0118-3. [PubMed: 17351841]
30. Hendley JO. Clinical practice. Otitis media. N Engl J Med. 2002; 347:1169–1174. doi:10.1056/ NEJMcp010944. [PubMed: 12374878]
31. Yu D, et al. An efficient recombination system for chromosome engineering in escherichia coli. Proc Natl.Acad.Sci.U.S.A. 2000; 97:5978–5983. [PubMed: 10811905]
32. Zhu Y, et al. Munc13-2-/- baseline secretion defect reveals source of oligomeric mucins in mouse airways. J Physiol. 2008; 586:1977–1992. [PubMed: 18258655]
33. Roy MG, et al. Mucin production during prenatal and postnatal murine lung development. Am J Respir Cell Mol Biol. 2011; 44:755–760. doi:10.1165/rcmb.2010-0020OC. [PubMed: 21653907]

34. Sisson JH, Stoner JA, Ammons BA, Wyatt TA. All-digital image capture and whole-field analysis of ciliary beat frequency. J Microsc. 2003; 211:103–111. [PubMed: 12887704]
35. Voronina VA, et al. Inactivation of chibby affects function of motile airway cilia. J Cell Biol. 2009; 185:225–233. doi:10.1083/jcb.200809144. [PubMed: 19364920]
36. Coote K, Nicholls A, Atherton HC, Sugar R, Danahay H. Mucociliary clearance is enhanced in rat models of cigarette smoke and lipopolysaccharide-induced lung disease. Experimental Lung Research. 2004; 30:59–71. [PubMed: 14967604]
37. You Y, Richer EJ, Huang T, Brody SL. Growth and differentiation of mouse tracheal epithelial cells: Selection of a proliferative population. Am J Physiol Lung Cell Mol.Physiol. 2002; 283:L1315–L1321. [PubMed: 12388377]
38. Dillard P, Wetsel RA, Drouin SM. Complement c3a regulates muc5ac expression by airway clara cells independently of th2 responses. Am J Respir Crit Care Med. 2007; 175:1250–1258. [PubMed: 17400733]
39. Matsui H, et al. Evidence for periciliary liquid layer depletion, not abnormal ion composition, in the pathogenesis of cystic fibrosis airways disease. Cell. 1998; 95:1005–1015. [PubMed: 9875854]
40. Okada SF, et al. Voltage-dependent anion channel-1 (vdac-1) contributes to atp release and cell volume regulation in murine cells. J Gen Physiol. 2004; 124:513–526. doi:10.1085/jgp.200409154. [PubMed: 15477379]
41. Weinberg ED. Iron withholding: A defense against infection and neoplasia. Physiol Rev. 1984; 64:65–102. [PubMed: 6420813]
42. Weinberg ED. Nutritional immunity. Host's attempt to withold iron from microbial invaders. JAMA. 1975; 231:39–41. [PubMed: 1243565]
43. Weinberg ED. Iron and susceptibility to infectious disease. Science. 1974; 184:952–956. [PubMed: 4596821]
44. Evans SE, et al. Stimulated innate resistance of lung epithelium protects mice broadly against bacteria and fungi. Am J Respir Cell Mol.Biol. 2009
45. DeSantis TZ, et al. Greengenes, a chimera-checked 16s rrna gene database and workbench compatible with arb. Appl Environ Microbiol. 2006; 72:5069–5072. doi:10.1128/AEM.03006-05. [PubMed: 16820507]
46. Drancourt M, et al. 16s ribosomal DNA sequence analysis of a large collection of environmental and clinical unidentifiable bacterial isolates. J Clin Microbiol. 2000; 38:3623–3630. [PubMed: 11015374]
47. Moghaddam SJ, et al. Haemophilus influenzae lysate induces aspects of the chronic obstructive pulmonary disease phenotype. Am J Respir Cell Mol.Biol. 2008; 38:629–638. [PubMed: 18096867]
48. Steinkamp JA, Wilson JS, Saunders GC, Stewart CC. Phagocytosis: Flow cytometric quantitation with fluorescent microspheres. Science. 1982; 215:64–66. [PubMed: 7053559]
49. Lozupone C, et al. Widespread colonization of the lung by tropheryma whipplei in hiv infection. Am J Respir Crit Care Med. 2013; 187:1110–1117. doi:10.1164/rccm.201211-2145OC. [PubMed: 23392441]
50. Moghaddam SJ, et al. Promotion of lung carcinogenesis by chronic obstructive pulmonary disease-like airway inflammation in a k-ras-induced mouse model. Am J Respir Cell Mol.Biol. 2009; 40:443–453. [PubMed: 18927348]
51. Evans CM, et al. Mucin is produced by clara cells in the proximal airways of antigen-challenged mice. Am J.Respir.Cell Mol.Biol. 2004; 31:382–394. [PubMed: 15191915]

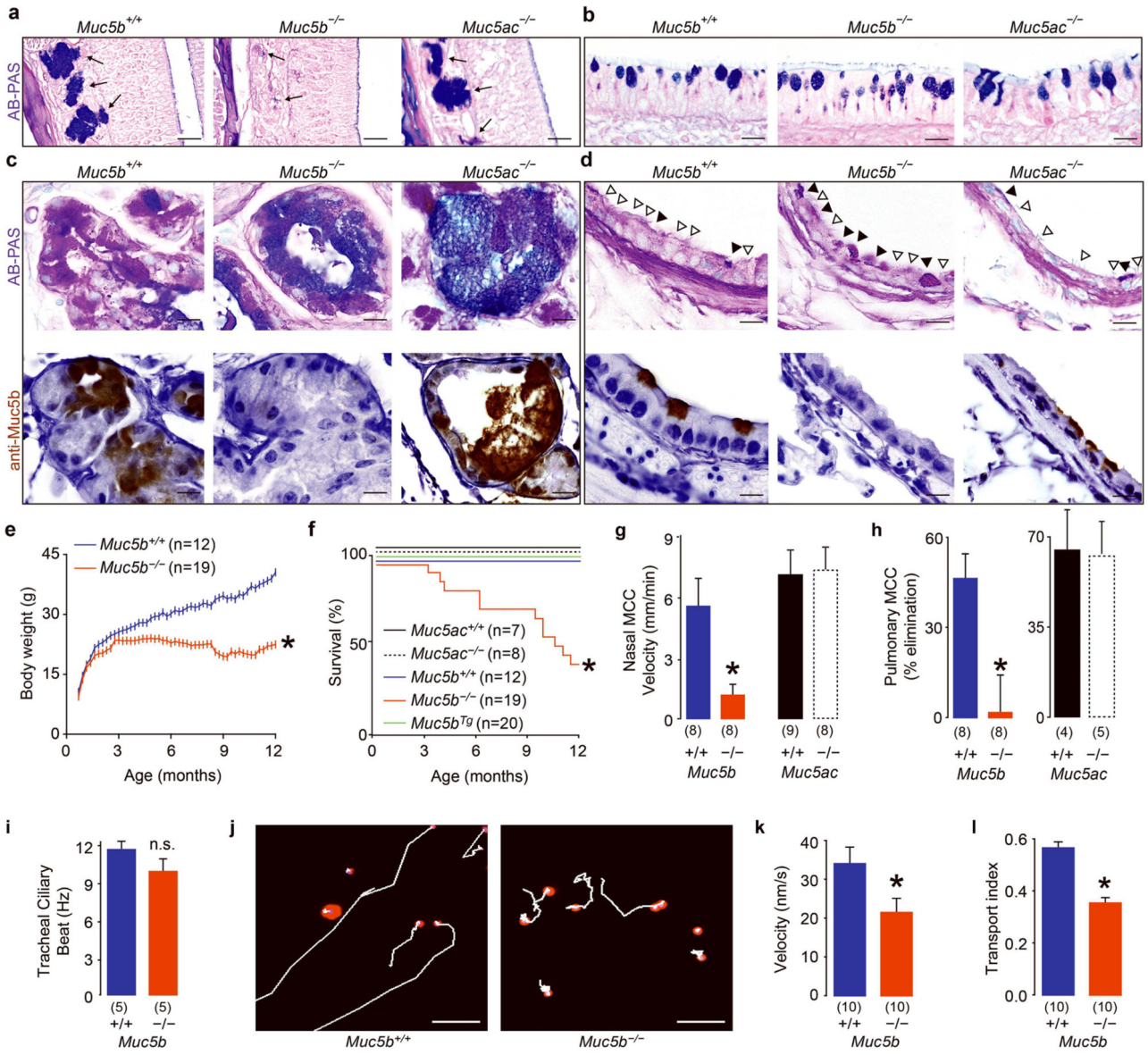

Figure. 1. Muc5b is required for survival and particle clearance

a-d, *Muc5b*$^{+/+}$, *Muc5b*$^{-/-}$, and *Muc5ac*$^{-/-}$ olfactory glands (**a**), nasopharynxes (**b**), tracheal glands (**c**), and bronchial surface epithelial cells (**d**) stained with AB-PAS or with anti-Muc5b (**c,d** bottom). Solid arrowheads, mucous cells. Open arrowheads, ciliated cells. **e-i**, Effects of mucin expression on growth, survival, MCC, and ciliary function. **j-l**, Microsphere movement, transport velocity, and transport index in primary tracheal epithelial cells *in vitro*. Scale bars, 20 μm (**a**, **j**), 10 μm (**b-d**). Error bars, sem. '*' significant differences ($p<0.05$). Numbers in parentheses, 'n' mice.

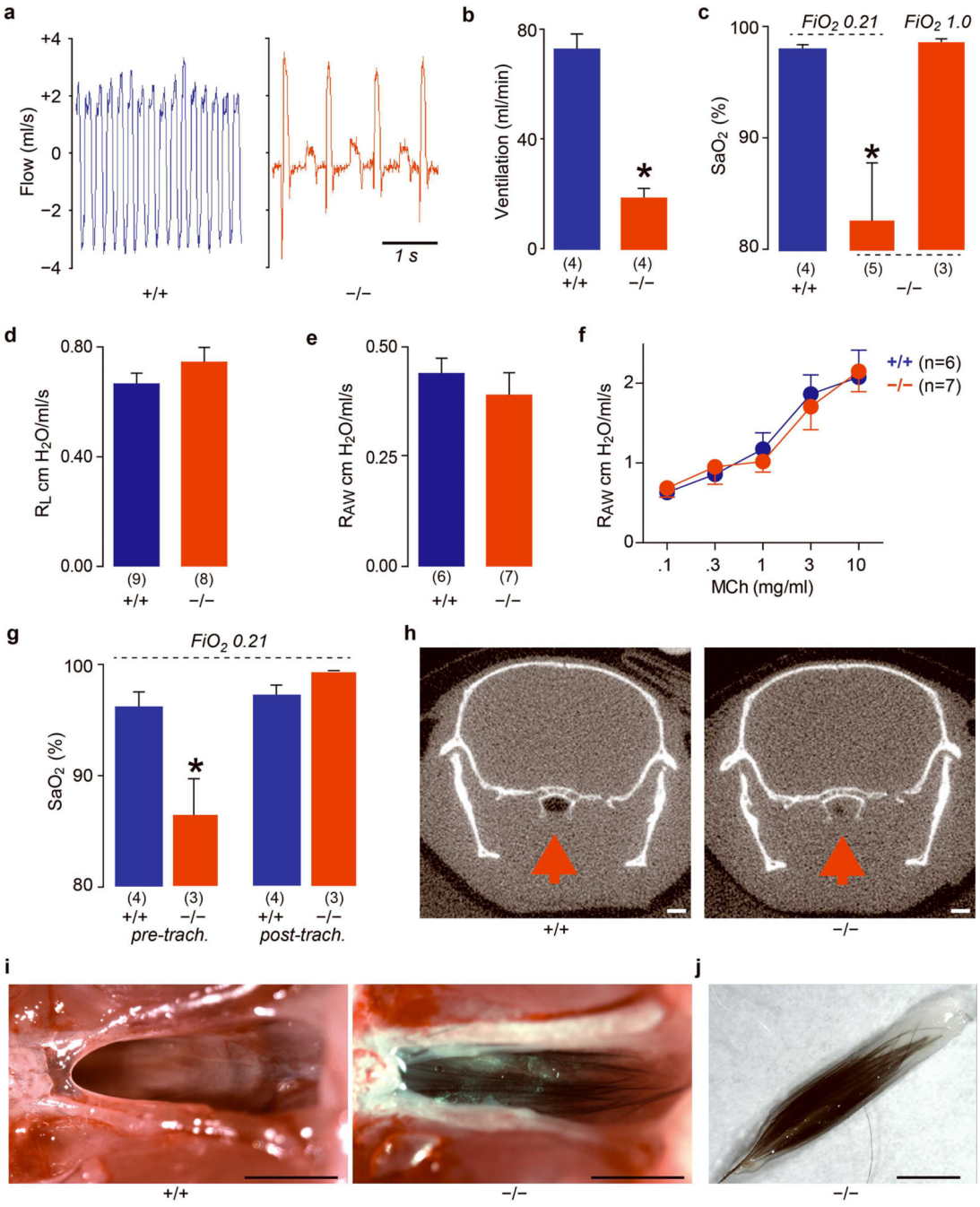

Figure. 2. Muc5b deficiency causes severe upper airway obstruction

a-b, Airflow and ventilation in *Muc5b*$^{+/+}$ and *Muc5b*$^{-/-}$ mice. **c**, Oxygen saturation (SaO_2) and rescue with 100% O_2 supplementation (FiO_2 1.0). **d-f**, Lung (R_L) and lower airway (R_{AW}) resistance and hyperresponsiveness to methacholine (MCh) in mechanically ventilated mice. **g**, Upper airway by-pass by tracheostomy under normoxia (FiO_2 0.21). **h**, Upper airway obstruction in *Muc5b*$^{-/-}$ mice confirmed by micro-CT (red arrows, nasopharynxes). **i,j**, Hair encased in mucus-like plugs visible during necropsy. Scale bars, 1 mm. Error bars, sem. '*', significant difference ($p<0.05$). Numbers in parentheses, 'n' mice.

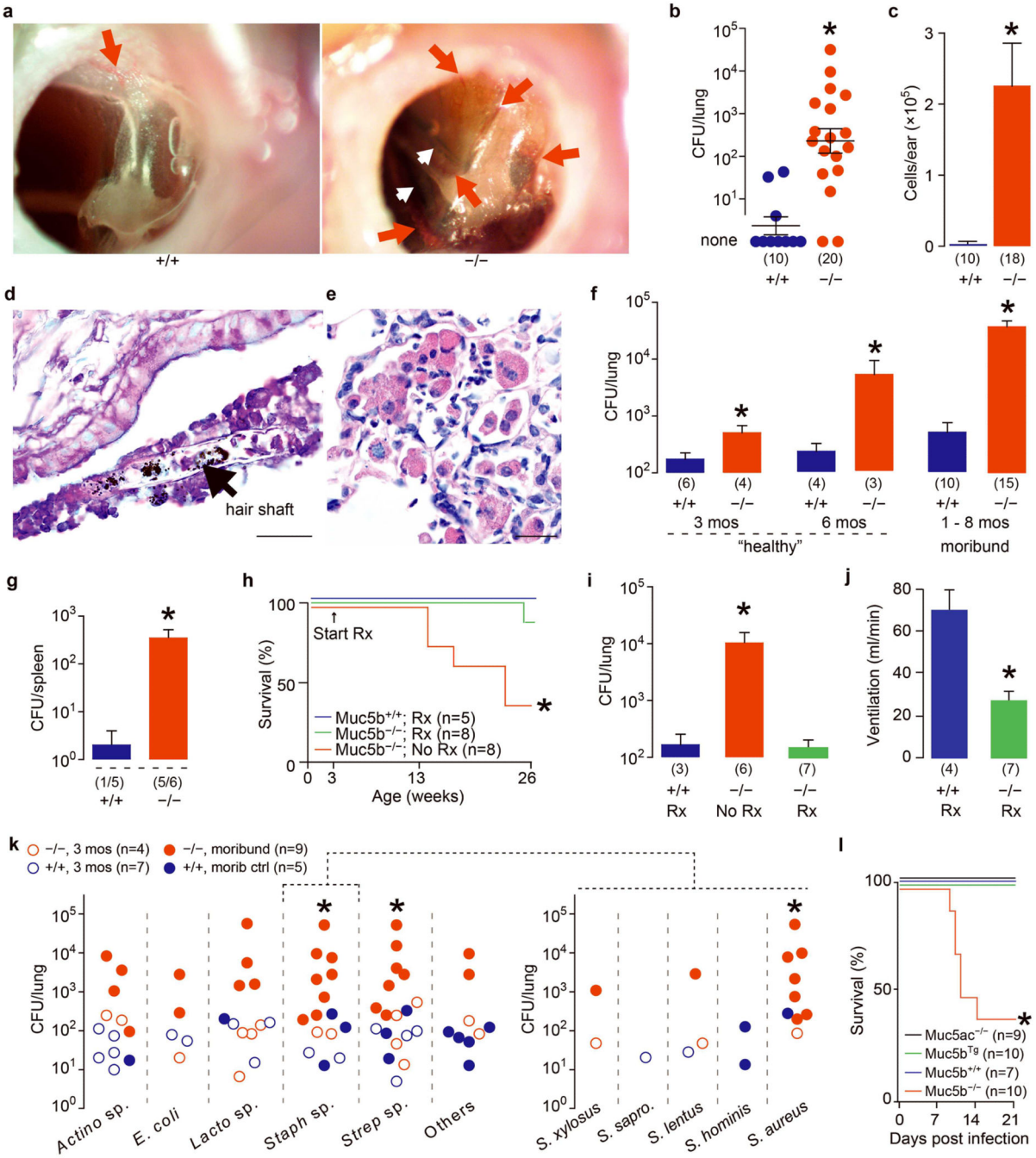

Figure. 3. Infection is the cause of death in *Muc5b*$^{-/-}$ mice

a-c, Hyperemic blood vessels (red arrows), hair (white arrows), bacteria, and leukocytes (>95% neutrophils) in *Muc5b*$^{-/-}$ middle ears. **d**,**e**, Hair fragments and leukocytes in *Muc5b*$^{-/-}$ lungs. **f**,**g**, Chronically accumulating bacteria in lungs, leading to moribundity and septicemia in *Muc5b*$^{-/-}$ mice. **h-j**, Mortality, infection, and ventilation with antibiotic treatment. **k**, Bacterial genera, and staphylococcal species in *Muc5b*$^{-/-}$ mice. **l**, Survival following intranasal *S. aureus* inoculation (10^7 CFU/mouse). Scale bars, 20 μm (**d**,**e**). Error bars, sem '*' statistical significance ($p<0.05$). Numbers in parentheses, 'n' mice.

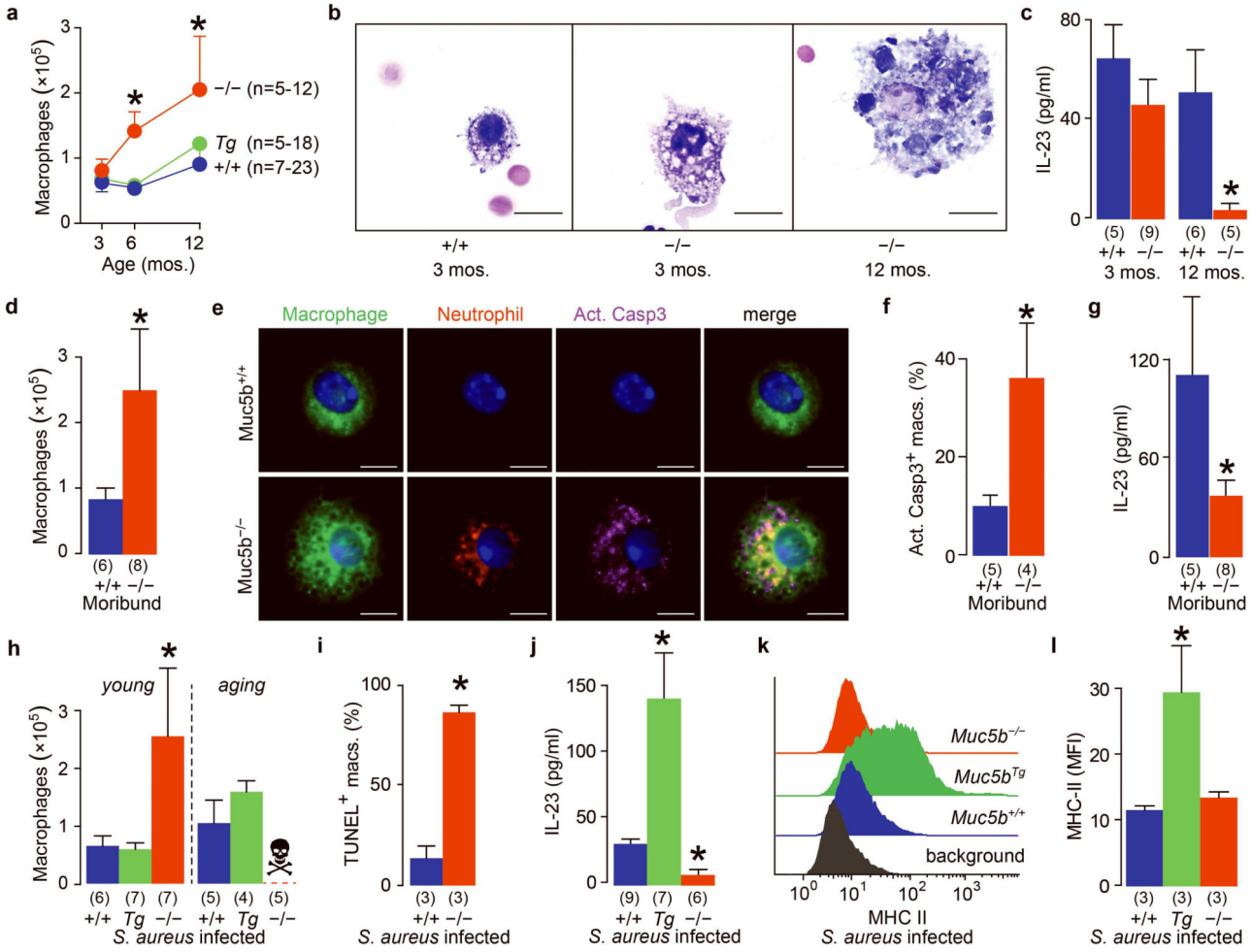

Figure. 4. Muc5b maintains functioning lung macrophage populations

a-c, Temporal changes in lung lavage macrophage numbers and morphologies and in IL-23. **d-g**, Macrophage numbers and apoptosis, and IL-23, in spontaneously moribund and control lungs. **h-j**, Macrophage numbers and apoptosis, and IL-23, in young (3 mos) and old (6-7 mos) lungs 7d after intratracheal USA300 infection (10^8 CFU/mouse). **j-l**, IL-23 and macrophage MHC-II in infected *Muc5b*^{Tg} mice. *Muc5b*^{Tg} lavage USA300 DNA was >98% reduced; incidence was 25% vs. 67% (*Muc5b*$^{+/+}$) and 100% (*Muc5b*$^{-/-}$), χ^2p=0.03. Error bars, sem. '*', statistical significance (p<0.05). Representative data in **k**. Numbers in parentheses, 'n' mice.